Dual Ratiometric Fluorescence Monitoring of Mechanical Polymer Chain Stretching and Subsequent Strain-Induced Crystallization

Kensuke Suga, Takuya Yamakado, and Shohei Saito*

Graduate School of Science, Kyoto University, Kitashirakawa Oiwake-cho, Sakyo-ku, Kyoto 606-8502, Japan.

KEYWORDS: force probe, mechanochemistry, strain-induced crystallization, dual emission, ratiometric imaging

ABSTRACT: Tracking the behavior of mechanochromic molecules provides valuable insights into force transmission and associated microstructural changes in soft materials under load. Herein, we report a dual ratiometric fluorescence (FL) analysis for monitoring both mechanical polymer chain stretching and strain-induced crystallization (SIC) of polymers. SIC has recently attracted renewed attention as an effective mechanism for improving the mechanical properties of polymers. A polyurethane (PU) film incorporating a trace of a dual-emissive flapping force probe (N-FLAP, 0.008 wt%) exhibited a blue-to-green FL spectral change in a low stress region (< 20 MPa), resulting from conformational planarization of the probe in mechanically stretched polymer chains. Only at higher probe concentrations (~0.65 wt%), the PU film showed a second spectral change from green to yellow during the SIC growth (20–65 MPa) due to self-absorption of scattered FL in a short wavelength region. The reversibility of these spectral changes was demonstrated by load-unload cycles. With these results in hand, the degrees of the polymer chain stretching and SIC were quantitatively mapped and monitored by dual ratiometric imaging based on different FL ratios (I_{525}/I_{470} and I_{525}/I_{600}). Simultaneous analysis of these two mappings revealed a spatio-temporal gap in the distribution of the polymer chain stretching and the SIC. The combinational use of the dual-emissive force probe and the ratiometric FL imaging is a universal approach for the development of soft matter physics.

INTRODUCTION

Mechanical properties of polymers are important in a wide range of applications,[1] such as shape memory materials,[2,3] self-healing materials,[4–8] stimuli-responsive materials,[9,10] photoswitching materials,[11–13] actuators,[14,15] functional adhesives,[16,17] wearable materials/devices,[18,19] and 3D printing fabrication leading to soft robotics and biomaterial engineering.[20–24] To effectively design and optimize the mechanical performance of these materials, it is crucial to have a comprehensive understanding of the force transmission at the molecular level and the resulting structural change of polymer network and polymer chains.[25–40] In addition to the classical studies,[41–44] these multi-scale investigations of the intricate relationship between stress and structure have revealed the fundamental principles governing the mechanical behavior of soft materials.

In relation to this, strain-induced crystallization (SIC) is an important physical property of polymers. Entropic reduction in stretched polymer chain conformations is predicted to cause anisotropic assembly of the polymer chains, leading to the formation of local crystalline structures. While the classical studies of SIC date back to the 1920s,[45–47] SIC is becoming a hot topic in recent materials science due to its essential role in the self-reinforcement mechanism of synthetic polymers[38,39] as well as natural rubber[48–50]. In these reports, SIC remarkably improves mechanical strength and fracture toughness, particularly resistance to crack propagation. To date, *in situ* FT-IR/WAXD/SAXS measurements are powerful tools for evaluating SIC based on the ordered structures of each segment in polymers (Figure 1a).[51–56] A recently developed digital image correlation (DIC) technique is also a good alternative.[57–60] However, it is still challenging to track nano- and microstructures simultaneously with the information of local forces on the stretched polymer chains.

On the other hand, the development of mechano-responsive molecules has contributed greatly to the fruitful mechanochemistry[61–68] and mechanobiology.[69–73] Some of these molecular units can detect and quantify the local forces in the pico- to nanonewton range. FRET (Förster resonance energy transfer)-based fluorescent force probes have been used to quantify forces of several to 50 pN applied to cellular systems.[74–76] Mechanophores can also visualize local forces in soft materials in the range of more than 200 pN because, in principle, intramolecular covalent bond scission is required for the mechanical responses.[77–80] In particular, mechanophores are useful from multiple perspectives, such as initiation of chemical reactions,[81–83] toughening of polymeric materials by energy dissipation,[84,85] induction of self-healing ability,[86] as well as the detection of single-chain force distribution,[30,87] polymer microstructural change including SIC[88–90], and material damage.[30,91,92] With these backgrounds, we have explored the force probing function[93–95] of conformationally flexible dual-emissive molecules, FLAP (flexible and aromatic photofunctional system).[96–98]

While several mechanochromic molecules have been reported with reversible responses,[99–108] the flapping

molecules (FLAP) are suitable for ratiometric fluorescence (FL) analysis on the distribution of nanoscale stress concentration in polymer chain network.[93,94] When incorporated into a polymer chain, FLAP with a central COT ring takes a relaxed bent form, emitting a blue FL. When the polymer chain is stretched, the bent conformation of FLAP is mechanically planarized to emit a green FL (Figure 1b). This conformational change does not require covalent bond scission. Therefore, the mechanical response is fully reversible and induced with a lower force threshold than conventional mechanophores, theoretically predicted to be around 100 pN. This force threshold is ideal for monitoring the polymer chain stretching prior to the mechanical failure, because the force range lies between the thermal fluctuations at room temperature (4.1 pN nm)[71,109] and the polymer chain cleavage including covalent mechanophore activation (more than 240 pN).[77,78] In addition, ratiometric FL imaging, which maps the ratio of FL intensity at two different wavelengths in each image pixel, can be performed for real-time evaluation of nanoscale stress distribution.

Here we report the optical monitoring of mechanical polymer chain stretching and subsequent SIC growth of segmented polyurethanes (PUs) in separated images based on a newly developed technique, that is, dual ratiometric FL analysis using a nitrogen-embedded flapping force probe (N-FLAP in Figure 1b). In addition to the mechanically induced bent-to-planar conformational change of the N-FLAP probe, a subsequent FL response was observed with the appearance of SIC under high stress (Figure 1c, Supporting Movie 1), resulting from a pronounced self-absorption of the scattering FL under SIC. The vivid two-step spectral evolution allows ratiometric spatiotemporal imaging of these two important events separately. Namely, the degrees of the polymer chain stretching and the subsequent SIC can be quantitatively mapped and monitored.

RESULTS AND DISCUSSION

Synthesis of the flexible dual-emissive force probe

As a conformationally flexible mechanoresponsive fluorophore, nitrogen-embedded FLAP (N-FLAP)[110] was selected for this study, which is reported as a more photostable fluorophore than a conventional anthracene-based FLAP.[97] The synthesis of N-FLAP was improved by using COT-fused *o*-phenylene diamine **1**[111] as a key precursor (Figure 2). Crystalline sample of **1** can be easily obtained as hydrochloride in gram scale, and the single-crystal X-ray structure analysis indicated the presence of four counter anions (Figure S5-1). Condensation of **1** and 2,5-dihydroxy-1,4-benzoquinone gave a COT-fused phenazine dimer **2** in 99% yield. S_N2 reaction of **2** with 1-bromohexane under basic condition yielded **N-FLAP1** in 45% yield. In this synthetic protocols, **N-FLAP1** can be synthesized and easily purified in 200–300-mg scale. **N-FLAP2** bearing four OH groups at the terminal positions was also synthesized from **2** in 41% yield, which can be chemically doped in polymers.

Before incorporating **N-FLAP2** into PUs, a model reaction was performed to confirm the reactivity of **N-FLAP2**. **N-FLAP2** was reacted with *p*-tolyl isocyanate to give **N-FLAP3** bearing four phenyl urethane units quantitatively, which supported the successful chemical doping in the following polymerization. These compounds were identified by ^{1}H and ^{13}C NMR analysis as well as high-resolution mass spectrometry (Figures S3-1 to S3-3 and S4-1 to S4-2).

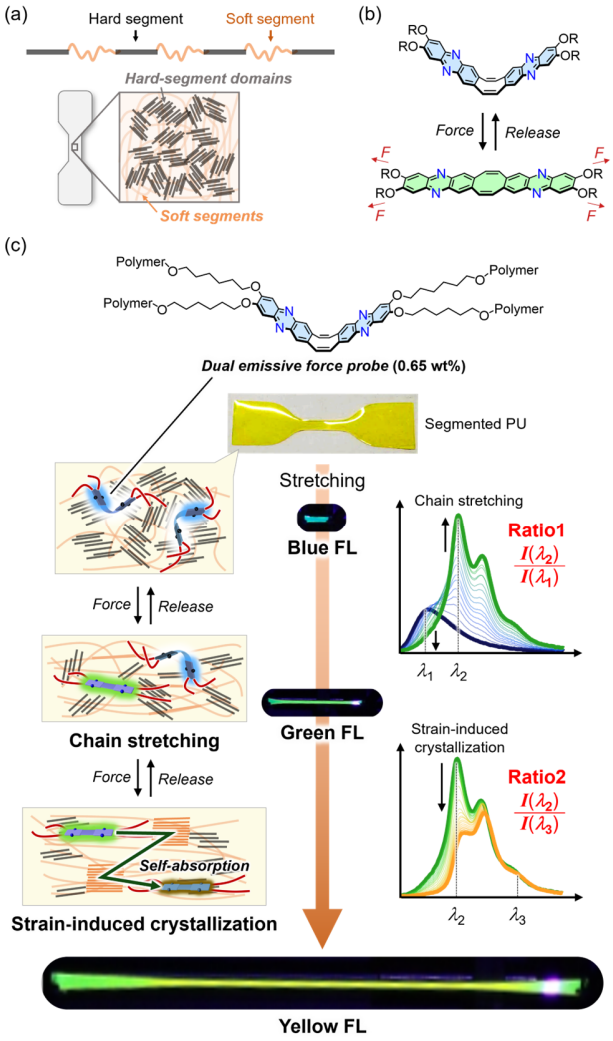

Figure 1 (a) Segmented polyurethane composed of hard segments and soft segments. (b) COT-fused flapping phenazine, N-FLAP, as a dual emissive force probe. (c) Concept for the two-step ratiometric monitoring of mechanical polymer chain stretching and subsequent strain-induced crystallization (SIC).

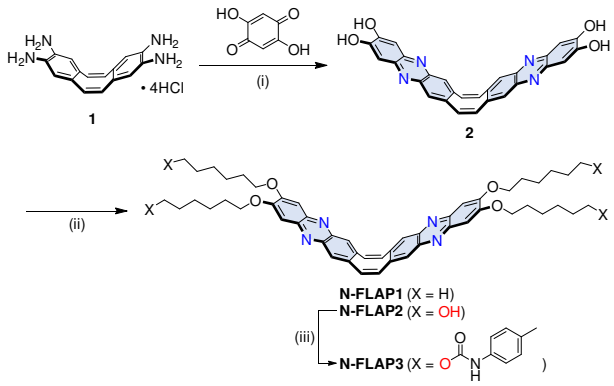

Figure 2. Synthesis of N-FLAP derivatives. Conditions: (i) H_2O, 100 °C, y. 99%; (ii) 1-bromohexane, DMF, 55 °C for **N-FLAP1**, y. 45%, and 6-bromo-1-hexanol, DMF, 40 °C for **N-FLAP2**, y. 41%; (iii) *p*-tolyl isocyanate, dibutyltin dilaurate (DBTDL), THF, 30 °C, y. 100%.

Synthesis and characterization of segmented PUs

Chemical doping of **N-FLAP2** into segmented PUs was performed using poly-(tetrahydrofuran) (PTHF, $M_n \approx$ 1,000), 4,4'-diphenylmethane diisocyanate (MDI), and 1,4-butanediol (BDO) as monomers. Two-step polymerization method was applied to obtain segmented PUs via a prepolymer (Figure 3), which is commonly used for incorporating various mechanophores.[94,104,112] In the first stage, **N-FLAP2** was copolymerized with MDI and PTHF to obtain prepolymers with different N-FLAP doping ratios. Then, BDO was added to prepare segmented PUs **PU1-008**, **PU1-073**, **PU1-210**, and **PU1-650** containing 0.008, 0.073, 0.21, and 0.65 wt% of **N-FLAP2**, respectively (Table S6-1). In **PU1**, **N-FLAP2** probe was introduced at the crosslinking points of the hard segment. As a control sample, segmented **PU0** without **N-FLAP2** was synthesized in the same way.

The molar ratio of the soft and hard segments was determined to be 1:(2.3–2.5) by the ^{1}H NMR analysis, which is consistent with the monomer ratio used for the reaction (Figures S6-4 to S6-8). Molecular weight of these PUs was estimated by SEC (Figure S6-3 and Table S6-3). Thermal properties of the synthetic PUs analyzed by differential scanning calorimetry (DSC, Figure S6-10) were similar to those of the previously reported PUs.[94] Since the glass transition temperature (T_g) of the soft segments was lower than room temperature, all tensile tests on the PUs were performed in the rubbery state. The number average molecular weights (M_n) of **PU0** and **PU1-008** were determined to be 66,100 and 55,400, respectively, which are comparable to similar PUs (M_n = 49,600–84,800).[94] On the other hand, the molecular weights of **PU1-074**, **PU1-210**, and **PU1-650** are significantly higher (Table S6-3), presumably due to the crosslinking effect by N-FLAP.

Environment-sensitive properties of the FL probe

Photophysical properties of urethane-capped **N-FLAP3** were measured in comparison with the reported **N-FLAP1**. In dichloromethane, the absorption and FL spectra were almost identical, and the molar absorption coefficient (ε) of **N-FLAP3** was 57,300 mol L^{-1} cm^{-1} at 414 nm, as high as that of **N-FLAP1** (Figure 4a). As previously reported,[96,110,111] the large Stokes shift (4900 cm^{-1}) indicated a dynamic bent-to-planar conformational change in the excited state (Figure 4d, Table S7-2). The FL quantum yield of **N-FLAP3** (Φ_F = 0.34) was a bit lower than that of **N-FLAP1** (Φ_F = 0.42), and the FL lifetime of **N-FLAP3** (τ_F = 2.1 ns, Figure S7-1d and Table S7-1) was slightly shorter than that of **N-FLAP1** (τ_F = 2.4 ns).[110] This result indicates that the presence of the phenyl urethane moieties contributes to a non-emissive decay, but the performance of the N-FLAP probe is in principle preserved.

An absorption band of the **PU1-650** film (Figure 4b) was observed at 418 nm, arising from chemically doped N-FLAP. The **PU1-650** films exhibited a blue FL (Φ_F = 0.028) with a peak at 484 nm, indicating that N-FLAP takes a bent conformation in the unstretched film, and the excited-state planarization is suppressed due to the small polymer free volume[110] (Figure 4c). On the other hand, a THF solution of **PU1-650** (*ca.* 0.2 g/L) showed a green FL band at 515 nm (Φ_F = 0.23), as similarly observed for the THF solution of **N-FLAP3**, indicating the excited-state planarization of the chemically doped N-FLAP probe spontaneously occurs in the solvated conditions.

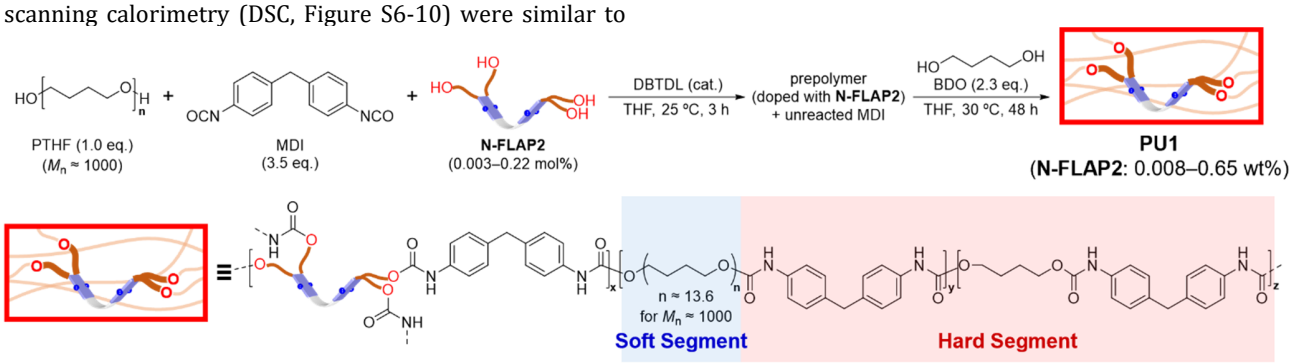

Figure 3. Synthesis and chemical structure of segmented polyurethane elastomers **PU1**, chemically doped with different amounts of **N-FLAP2**.

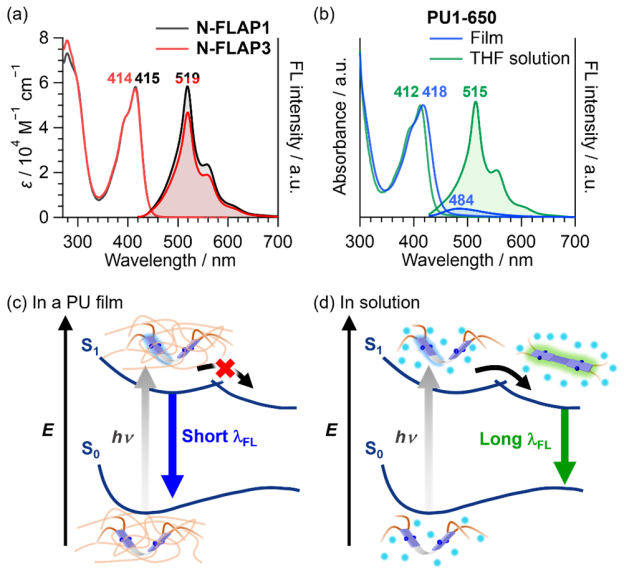

Figure 4. UV-visible absorption and FL spectra (λ_{ex} = 415 nm) of (a) **N-FLAP3** in comparison to **N-FLAP1** in CH_2Cl_2, and of (b) **PU1-650** in the film state and in a THF solution. **PU1-650** means the PU1 elastomer chemically incorporated with 0.65 wt% of **FLAP2**. (c, d) Different excited-state dynamics of the N-FLAP probe in polymers in the absence/presence of solvent molecules.

Tensile stretching and simultaneous FL measurement

Uniaxial stretching of the prepared PU specimen was performed, monitoring the FL spectrum at the central position of the stretched film. The obtained stress–strain curves were comparable among the synthesized PUs (**PU0**, **PU1-008**, **PU1-074**, **PU1-210**, and **PU1-650**) and the previously reported PU[94] (Figure 5a and Figure S8-1), in spite of the different molecular weights. As previously demonstrated in the other FLAPs, we expected that N-FLAP also showed a similar blue-to-green FL change, when the PU elastomers were gradually stretched. Namely, the chemically doped N-FLAP probe would be mechanically stretched from the bent to the planar form in the S_0 ground state by local forces transmitted in polymer chains (Figure 5b).

The prediction was true for **PU1-008** (Figure 5c). Up to the fracture point of the specimen (strain: *ca.* 600%, stress: *ca.* 60 MPa), the obtained stress-strain curve can be divided into several regions, depending on the degree of strain at each stage. In the elastic region (strain: 0 to 8%, stress: 0–6 MPa), the blue FL spectra did not change, indicating that the N-FLAP probe maintains its bent form. In the plateau-like region (strain: 8 to 100%, stress: 6–10 MPa), the blue FL (472 nm) of the bent N-FLAP started to decrease, and the green FL (522 nm) of the planar form concomitantly increased. Then, in the beginning of the strain-hardening region (strain: 100 to 280%, stress: 10–20 MPa), a remarkable blue-to-green FL change has evolved. This spectral change was almost saturated up to 440% strain (40 MPa stress), where the blue FL band practically disappeared and the green FL band with vibronic structures was mainly observed. Accordingly, a new absorption band has evolved at 520 nm under 40 MPa, which was assigned to the lowest energy excitation of the planarized conformation of N-FLAP (see the next Section and Figure S9-2). It is worth noting that the average intermolecular distance of the FL probe in **PU1-008** was calculated to be 26 nm, assuming homogeneous dispersion (Table S6-2). This value is larger than the intermolecular distance at which Förster resonance energy transfer (FRET) can occur (< 10 nm). Therefore, a spectral perturbation by FRET can be excluded at least for the blue-to-green process in **PU1-008**.

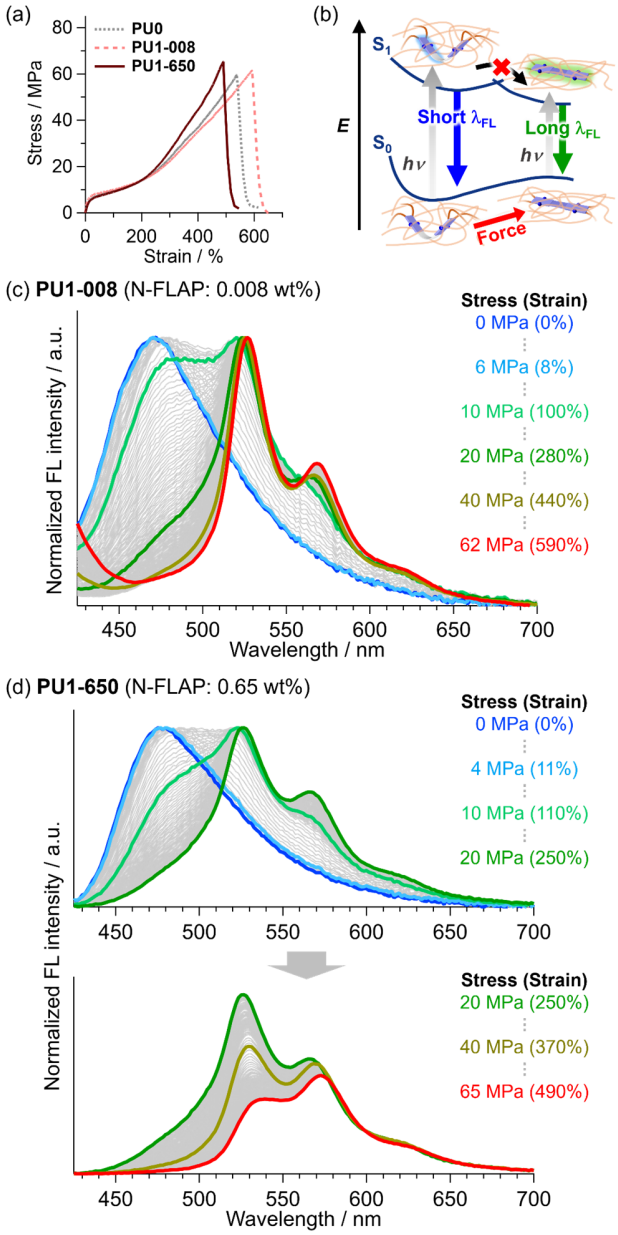

Figure 5. (a) Stress–strain curves of synthesized segmented polyurethanes **PU0**, **PU1-008**, and **PU1-650**. See Figure S8-1 for the other PUs. (b) Mechanism of the mechanically induced FL spectral change of N-FLAP. (c,d) FL spectral monitoring of (c) **PU1-008** and (d) **PU1-650** during tensile tests. A two-step spectral change (0–20 MPa and 20–65 MPa) was observed for **PU1-650**.

On the other hand, the blue-to-green change was followed by an unexpected green-to-yellow FL color change in **PU1-650** under high stress over 20 MPa (Figure 5d and Supporting Movie 1), in which the relative FL intensity of the green band has significantly decreased. Among **PU1-008**, **PU1-074**, **PU1-210**, and **PU1-650**, the second spectral change became more pronounced as the N-FLAP concentration increased (Figures S8-2). Even when the strain rate was increased from 0.067 s^{-1} to 0.17 s^{-1}, there was virtually no change in the stress-strain curve and FL spectral evolution (Figures S8-1 and S8-5). To elucidate the mechanism of the second FL response, several experiments were performed below, and we found that SIC should be an important trigger.

Strain-induced crystallization and enhanced self-absorption

During the tensile tests, SIC was observed under high stress. The synthesized PUs were initially transparent, but these samples started to cloud when stretched over a certain strain (Figure 6a). This clouding is typically observed in segmented copolymers and it was attributed to SIC of the soft segments.[88] Indeed, the intensity of the scattered excitation light has suddenly increased at the late stage of the stretching tests (Figures S8-6a–d), for example at 370% strain (~40 MPa stress) in **PU1-650**. Interestingly, the plots of the FL intensity ratio (I_{525}/I_{600}) dropped significantly at the same strain (Figures 6b and S8-6e–h), although the small decrease has been also confirmed up to this point. This decrease was not observed in **PU1-008** (at the low concentration of the probe). We then assume that as more N-FLAP probes are mechanically planarized, the self-absorption of the green FL becomes pronounced in the stretched **PU1-650**, and the growing of SIC accelerates the degree of the self-absorption by internal scattering of the FL emission. Consistent with this assumption, an absorption band at 520 nm (theoretically assigned to a HOMO-LUMO transition of the planarized N-FLAP (Figure S9-2)) appeared and gradually evolved up to 370% strain (~40 MPa stress), while the unstretched film showed only short wavelength absorption below 500 nm due to the relaxed bent conformation of N-FLAP (Figure 6c). In addition, after SIC took place, the internal light scattering reaching 570 nm became pronounced. Spectral matching for the reabsorption of the green FL at 525 nm was demonstrated in Figure 6d, in which the decrease of the short wavelength FL was remarkable.

The mechanism of the FL spectral perturbation by SIC is illustrated in Figures 7a and 7b. In the high strain region, polymer chains of the soft segments begin to align along the stretching direction, promoting local crystallization. Once the crystalline domains are seeded, the domain size increases to several hundred nanometers and therefore the light scattering begins to be observed. Inside the polymer film, the scattering increases the mean random path length of the FL emission before FL reaches the surface.[113] At the low probe concentration (**PU1-008**), the scattering has no influence on the FL ratio of I_{525}/I_{600} due to the negligible effect of the FL reabsorption (Figure 7a). On the other hand, at the high probe concentration (**PU1-650**), a dramatic decrease in the same FL ratio is induced due to the significant self-absorption enhanced by SIC (Figure 7b). To support this explanation, we measured the FL lifetimes of each FL band in the stressed state. By freezing the stretched **PU1-650** samples with liquid N_2, the low and high stressed states were fixed before relaxation (Figure 7c). In both states, the emissive bands at 525 nm (τ_F = 3.0–3.8 ns) and at 575 nm (τ_F = 3.7–4.4 ns) showed a similar FL lifetime regardless of the relative intensities, while the blue FL at 475 nm (emitted from the bent N-FLAP) has a significantly shorter lifetime (Figure 7d and 7e). This result indicates that the two FL bands at 525 and 575 nm arise from the same species, that is, the planarized N-FLAP.

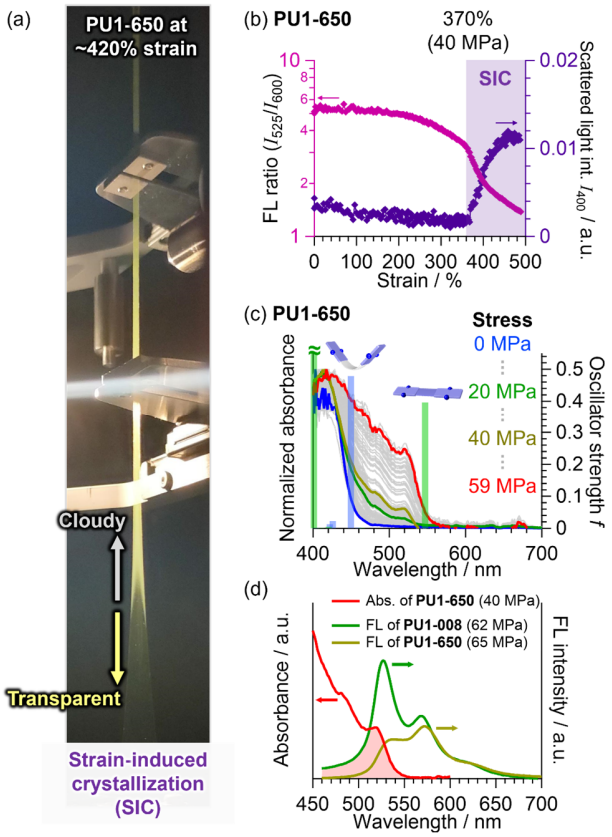

Figure 6. (a) Strain-induced crystallization of the stretched **PU1-650** film, observed at 420% strain. (b) Intensity of the scattered light at 400 nm (blue dots) and the FL ratio of I_{525}/I_{600} (purple dots) plotted against nominal strain in the tensile tests. Strain rate: 0.067 s^{-1}. (c) Visible absorption/scattering spectra of stretched **PU1-650**. Calculated excitation energies of the bent form (blue bars) and the planarized form (green bars) of N-FLAP have been shown with respective oscillator strengths (See Figure S9-2 for details). (d) Spectral overlap around 525 nm in the absorption and FL spectra of stretched **PU1-650**.

Ratiometric FL analysis in the reversible SIC

The observed two-step FL responses for different events (chain stretching and SIC) are useful to obtain quantitative information of nano-to-microscopic polymer structural changes. Namely, monitoring of the two different FL ratios of I_{525}/I_{472} (Figure 8a) and I_{525}/I_{600} (Figure 8b) enables "dual ratiometric analysis" for providing a valuable insight into polymer physics, which would be a complementary approach to the established techniques such as FTIR/WAXD/SAXS. For example, in Figure 8a, a small

difference in the monotonically increased FL ratios of I_{525}/I_{472} between **PU1-073**, **PU1-210**, and **PU1-650** suggests that the relative percentages of mechanically stressed N-FLAP crosslinkers are almost comparable at the same strain, despite the difference in the polymer molecular weights (Table S6-3). In addition, when SIC occurs at the inflection point of the I_{525}/I_{600} ratio in **PU1-210** and **PU1-650** (Figure 8b), the chain stretching at the most of crosslinkers have already done at the corresponding strain.

Furthermore, we employed this method to study reversible SIC[51] (Figure 8c) and thermal melting of SIC[114] (Figure 8d). When **PU1-650** was applied to the 11 times repeated cycles of load (50 MPa) and unload (0 MPa), the change in both the FL ratios was reversible throughout the cycle test (Figure 8c). The FL spectrum of the relaxed state was slightly red-shifted with increasing number of cycles, which is presumably due to small structural hysteresis of the crystalline soft segments. In this experiment, it takes only 38 s for the single cycle, indicating that conformational entropy of the polymer chains are smoothly recovered in the reversible SIC. In the heating test (Figure 8d), **PU1-650** was stretched to 475% strain, held at this strain for 30 s, and then heated using a blow dryer while maintaining the 475% strain. The sample temperature measured by a thermography camera increased from 27–28 °C to approximately 40°C by heating (Figure 8f). As a result, the cloudy sample immediately turned to be soft and transparent, just after the heating. Accordingly, the scattered intensity of the excitation light (purple line in Figure 8d) suddenly decreased and the FL ratio of I_{525}/I_{600} (red line) went back to the value before SIC, supporting the thermal melting of SIC domains. The concomitant decrease of the FL ratio of I_{525}/I_{472} (blue line) suggested the increased population of the relaxed N-FLAP probe. Namely, nanoscopic polymer chain entropy was increased with the melting of the microscopic crystalline phase.

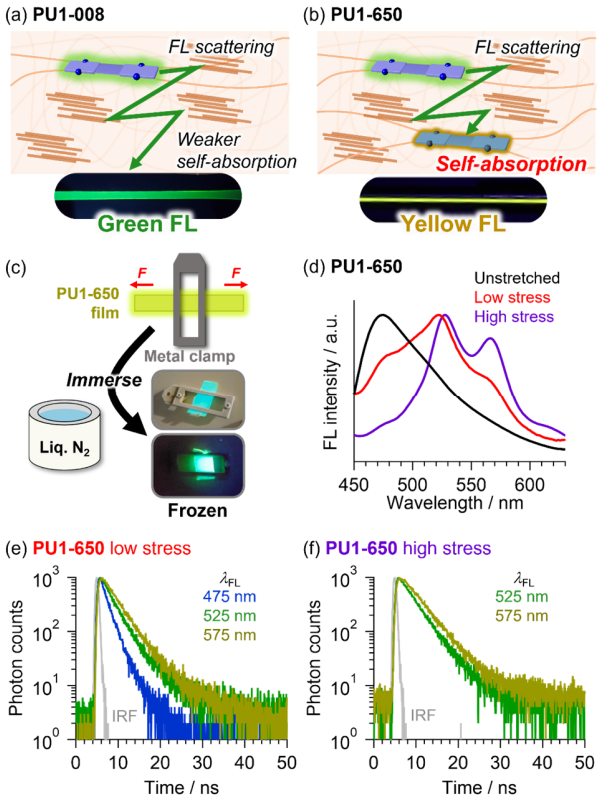

Figure 7. (a,b) Illustration of SIC and the scattering of FL for (a) **PU1-008** and (b) **PU1-650**. (c) Freezing of (un)stretched **PU-650** samples with liquid N_2 and the obtained FL spectra. λ_{ex} = 365 nm. (d,e) FL lifetimes of each FL band in frozen **PU1-650** samples under low and high stressed states. The measurements were performed at –195 °C. λ_{ex} = 405 nm.

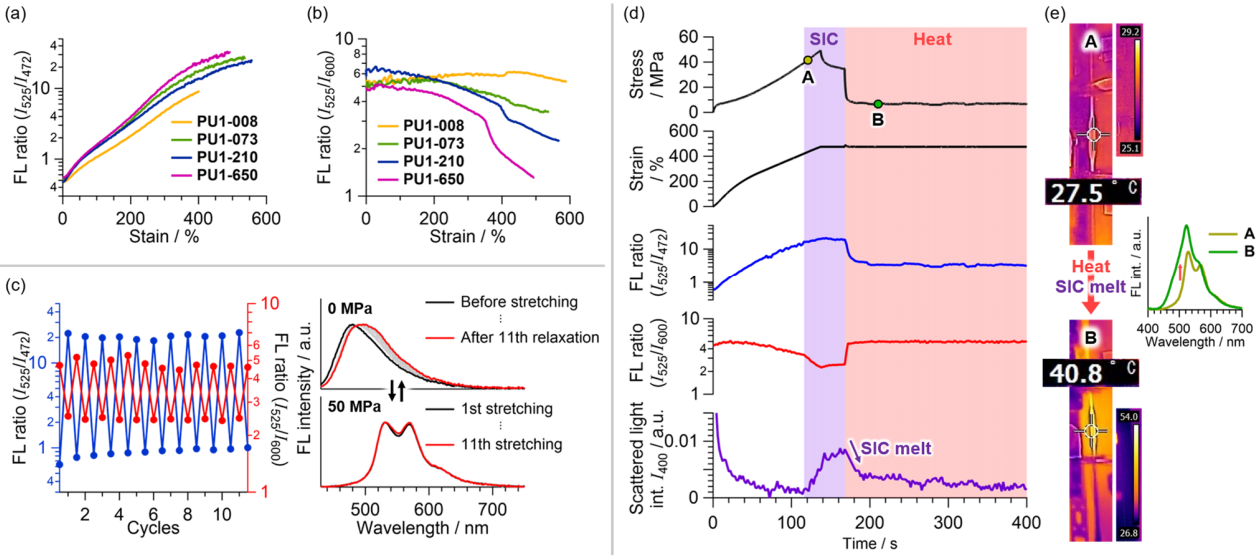

Figure 8. (a,b) Different FL ratio plots of (a) I_{525}/I_{472} and (b) I_{525}/I_{600} in the tensile tests of PUs with varied N-FLAP concentration. (c) Reversible responses in both FL ratios of **PU1-650** during 11 cycles between 0 MPa and 50 MPa. Strain rate: 0.67 s^{-1}. (d,e) A heating test to melt the SIC domains of **PU1-650** under the fixed strain of 475%. (d) Stress, strain, the two FL ratios, and the scattered excitation light intensity were plotted. Note that stress relaxation started with the fixed strain, and then the stress rapidly dropped by the thermal SIC melt. (e) Thermography analysis of the sample temperature as well as the FL spectra (inset) before and during heating (A and B, respectively). λ_{ex} = 365 nm.

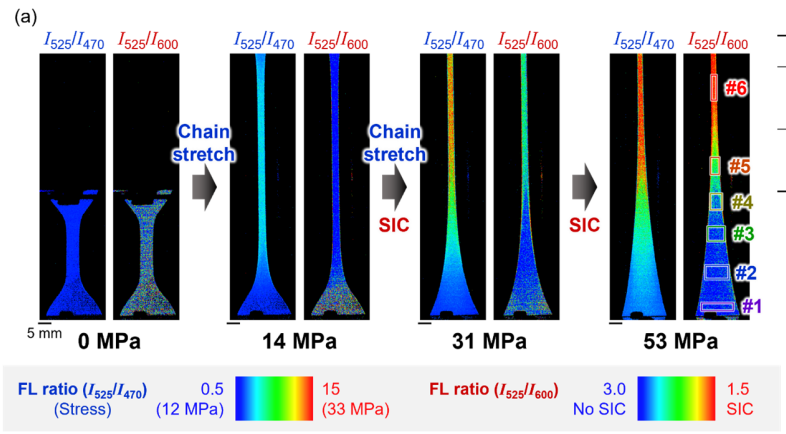

(b)

Area	#1	#2	#3	#4	#5	#6
FL ratio (I_{525}/I_{470})	3.3	4.6	7.5	11.1	19.1	22.4
Stress / MPa[a]	13	16	21	27	39	43
FL ratio (I_{525}/I_{600})	4.1	3.9	3.6	3.1	2.6	1.8
SIC[b]	–	–	–	–	in part	complete

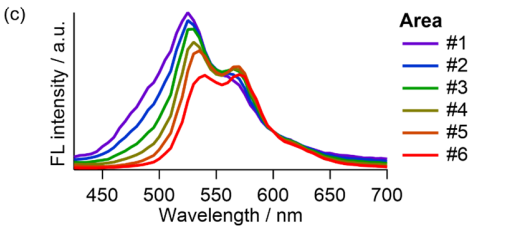

Figure 9. Real-time stress mapping of segmented PU elastomers by ratiometric FL imaging. (a) FL ratio mapping of a **PU1-650** specimen. Nominal stresses at the central position were measured by the tensile tester. These images were acquired using a hyperspectral camera. Two ratios (I_{525}/I_{470} and I_{525}/I_{600}) were adopted to detect chain stretching and SIC, respectively. Strain rate: 0.4 min^{-1}. Six different areas #1–6 are shown in the right figure. (b) Ratiometric analysis for each area. [a]Local stresses in each area were estimated from the obtained FL ratio (I_{525}/I_{470}), using a calibration curve prepared in advance for **PU1-650** (Figure S8-9). [b]Areas with the FL ratio (I_{525}/I_{600}) of less than 3.0 were judged to be the areas where SIC occurred. The threshold was determined from Figure 8b. (c) Averaged FL spectra for the selected areas in Figure 9a.

Dual ratiometric imaging to monitor the distribution of chain stretching and SIC

Finally, dual ratiometric FL imaging of the stretched **PU1-650** film was performed using a hyperspectral camera (Figure 9a). The values of the two FL ratios (I_{525}/I_{470} and I_{525}/I_{600}) were obtained at each pixel of the images, and the distribution was visualized in a combined movie (Supporting Movie 2). The two FL ratios can be considered to represent the chain stretching at the crosslinker and the SIC of the soft segment, respectively. From the spectrum of a selected area, the degrees of the chain stretching and the SIC can be separately evaluated at the same time (Figure 9b). Importantly, the analysis showed that there is a significant timing gap between the beginning of the chain stretching (at the crosslinkers) and the onset of SIC at the soft segments. In other words, these are stepwise events rather than simultaneous phenomena. To the best of our knowledge, this fact has only been demonstrated for polyethylene terephthalate (PET) based on the analyses of DSC and polarized FT-IR after drawing specimens,[115] which is easy to measure due to its high glass transition temperature (~342 K). The optical setup for the ratiometric imaging is universal, allowing the real-time analysis of low-T_g polymers under load.

CONCLUSIONS

In conclusion, we have demonstrated dual ratiometric fluorescence (FL) analysis on mechanical polymer chain stretching and subsequent strain-induced crystallization (SIC) in stressed soft materials. The ratiometric flapping force probe N-FLAP was chemically incorporated into crosslinking positions of segmented polyurethanes (PUs) at different concentrations (0.008–0.65 wt%). The stretched PU film showed a blue-to-green FL color change under low stress (below 20 MPa) in response to the polymer chain stretching. In addition, the PU film with 0.65 wt% of N-FLAP exhibited a subsequent green-to-yellow FL color change under higher stress up to 65 MPa. Spectral analysis revealed that the second spectral change occurs simultaneously with the SIC of the segmented PU. Through multiple experiments for mechanistic elucidation, the second response was attributed to the effect of self-absorption of the scattered FL in the crystallized PU. The spectral reversibility for both steps was confirmed by loading–unloading cycles. Dual ratiometric FL analysis based on the values of I_{525}/I_{470} and I_{525}/I_{600} has been developed to monitor the extent of fully stretched polymer chains and the subsequent SIC separately. This analytic approach has the obvious advantages in simultaneous *in-situ* observation of these two events based on the simple optical setup with excellent sensitivity and thickness independence. As a result, stepwise occurrence of the polymer chain stretching and the SIC has been experimentally demonstrated for rubbery PUs. Dual ratiometric FL imaging is a powerful tool for time- and space-resolved evaluation of the nano- and microscopic structural information in a wide range of soft materials under stress. Therefore, this strategy can be used to analyze and design tough polymers with improved mechanical properties by SIC. Furthermore, a combination of this method with the 3D printing technology will open up new possibilities for tailor-made 3D structural design with solid understanding.

ASSOCIATED CONTENT

Supporting Information

The Supporting Information is available free of charge on the ACS Publications website.

Experimental and theoretical details (PDF)
Movie S1 showing the two-step spectral response of **PU1-650** film under UV light and ambient light (MP4)
Movie S2 showing the dual ratiometric FL imaging of the mechanical polymer chain stretching and the strain-induced crystallization in **PU1-650** film (MP4)

Accession Codes

CCDC 2084063 contains the supplementary crystallographic data for this paper. These data can be obtained free of charge via www.ccdc.cam.ac.uk/data_request/cif, or by emailing data_request@ccdc.cam.ac.uk, or by contacting The Cambridge Crystallographic Data Centre, 12 Union Road, Cambridge CB2 1EZ, UK; fax: +44 1223 336033.

AUTHOR INFORMATION

Corresponding Author

* Shohei Saito: saito.shohei.4c@kyoto-u.ac.jp

Authors

Kensuke Suga
Takuya Yamakado

Notes

The authors declare no competing financial interest.

ACKNOWLEDGMENT

This work was supported by JST FOREST Program (Grant Number JPMJFR201L, Japan), JSPS KAKENHI (Grant Number JP21H01917, Japan), and JSPS fellowship (Grant Number JP22J21715 and 22KJ1964, Japan). We thank Prof. Dr. Hideki Yorimitsu for his help with high-resolution mass spectrometry measurements.

REFERENCES

(1) Zhao, X.; Chen, X.; Yuk, H.; Lin, S.; Liu, X.; Parada, G. Soft Materials by Design: Unconventional Polymer Networks Give Extreme Properties. *Chem. Rev.* **2021**, *121* (8), 4309–4372.

(2) Chan, B. Q. Y.; Low, Z. W. K.; Heng, S. J. W.; Chan, S. Y.; Owh, C.; Loh, X. J. Recent Advances in Shape Memory Soft Materials for Biomedical Applications. *ACS Appl. Mater. Interfaces* **2016**, *8* (16), 10070–10087.

(3) Lendlein, A.; Kelch, S. Shape-Memory Polymers. *Angew. Chem. Int. Ed.* **2002**, *41* (12), 2035–2057.

(4) Li, C.-H.; Zuo, J.-L. Self-Healing Polymers Based on Coordination Bonds. *Adv. Mater.* **2020**, *32* (27), e1903762.

(5) Wang, S.; Urban, M. W. Self-Healing Polymers. *Nat. Rev. Mater.* **2020**, *5* (8), 562–583.

(6) Burnworth, M.; Tang, L.; Kumpfer, J. R.; Duncan, A. J.; Beyer, F. L.; Fiore, G. L.; Rowan, S. J.; Weder, C. Optically Healable Supramolecular Polymers. *Nature* **2011**, *472* (7343), 334–337.

(7) Blaiszik, B. J.; Kramer, S. L. B.; Olugebefola, S. C.; Moore, J. S.; Sottos, N. R.; White, S. R. Self-Healing Polymers and Composites. *Annu. Rev. Mater. Res.* **2010**, *40* (1), 179–211.

(8) White, S. R.; Sottos, N. R.; Geubelle, P. H.; Moore, J. S.; Kessler, M. R.; Sriram, S. R.; Brown, E. N.; Viswanathan, S. Autonomic Healing of Polymer Composites. *Nature* **2001**, *409* (6822), 794–797.

(9) Wojtecki, R. J.; Meador, M. A.; Rowan, S. J. Using the Dynamic Bond to Access Macroscopically Responsive Structurally Dynamic Polymers. *Nat. Mater.* **2011**, *10* (1), 14–27.

(10) Capadona, J. R.; Shanmuganathan, K.; Tyler, D. J.; Rowan, S. J.; Weder, C. Stimuli-Responsive Polymer Nanocomposites Inspired by the Sea Cucumber Dermis. *Science* **2008**, *319* (5868), 1370–1374.

(11) Goulet-Hanssens, A.; Eisenreich, F.; Hecht, S. Enlightening Materials with Photoswitches. *Adv. Mater.* **2020**, *32* (20), e1905966.

(12) Irie, M.; Fukaminato, T.; Matsuda, K.; Kobatake, S. Photochromism of Diarylethene Molecules and Crystals: Memories, Switches, and Actuators. *Chem. Rev.* **2014**, *114* (24), 12174–12277.

(13) Priimagi, A.; Barrett, C. J.; Shishido, A. Recent Twists in Photoactuation and Photoalignment Control. *J. Mater. Chem. C* **2014**, *2* (35), 7155–7162.

(14) Martins, P.; Correia, D. M.; Correia, V.; Lanceros-Mendez, S. Polymer-Based Actuators: Back to the Future. *Phys. Chem. Chem. Phys.* **2020**, *22* (27), 15163–15182.

(15) Ionov, L. Polymeric Actuators. *Langmuir* **2015**, *31* (18), 5015–5024.

(16) Creton, C.; Ciccotti, M. Fracture and Adhesion of Soft Materials: A Review. *Rep. Prog. Phys.* **2016**, *79* (4), 046601.

(17) Hohl, D. K.; Weder, C. (DE)Bonding on Demand with Optically Switchable Adhesives. *Adv. Opt. Mater.* **2019**, *7* (16), 1900230.

(18) Nguyen, P. Q.; Soenksen, L. R.; Donghia, N. M.; Angenent-Mari, N. M.; de Puig, H.; Huang, A.; Lee, R.; Slomovic, S.; Galbersanini, T.; Lansberry, G.; Sallum, H. M.; Zhao, E. M.; Niemi, J. B.; Collins, J. J. Wearable Materials with Embedded Synthetic Biology Sensors for Biomolecule Detection. *Nat. Biotechnol.* **2021**, *39* (11), 1366–1374.

(19) Lim, H.-R.; Kim, H. S.; Qazi, R.; Kwon, Y.-T.; Jeong, J.-W.; Yeo, W.-H. Advanced Soft Materials, Sensor Integrations, and Applications of Wearable Flexible Hybrid Electronics in Healthcare, Energy, and Environment. *Adv. Mater.* **2020**, *32* (15), e1901924.

(20) Bagheri, A.; Fellows, C. M.; Boyer, C. Reversible Deactivation Radical Polymerization: From Polymer Network Synthesis to 3D Printing. *Adv. Sci.* **2021**, *8* (5), 2003701.

(21) Zhou, L.-Y.; Fu, J.; He, Y. A Review of 3D Printing Technologies for Soft Polymer Materials. *Adv. Funct. Mater.* **2020**, *30* (28), 2000187.

(22) Regehly, M.; Garmshausen, Y.; Reuter, M.; König, N. F.; Israel, E.; Kelly, D. P.; Chou, C.-Y.; Koch, K.; Asfari, B.; Hecht, S. Xolography for Linear Volumetric 3D Printing. *Nature* **2020**, *588* (7839), 620–624.

(23) Li, S.; Bai, H.; Shepherd, R. F.; Zhao, H. Bio-Inspired Design and Additive Manufacturing of Soft Materials, Machines, Robots, and Haptic Interfaces. *Angew. Chem. Int. Ed.* **2019**, *58* (33), 11182–11204.

(24) Wallin, T. J.; Pikul, J.; Shepherd, R. F. 3D Printing of Soft Robotic Systems. *Nat. Rev. Mater.* **2018**, *3* (6), 84–100.

(25) Okumura, Y.; Ito, K. The Polyrotaxane Gel: A Topological Gel by Figure-of-Eight Cross-Links. *Adv. Mater.* **2001**, *13* (7), 485–487.

(26) Gong, J. P.; Katsuyama, Y.; Kurokawa, T.; Osada, Y. Double-Network Hydrogels with Extremely High Mechanical Strength. *Adv. Mater.* **2003**, *15* (14), 1155–1158.

(27) Webber, R. E.; Creton, C.; Brown, H. R.; Gong, J. P. Large Strain Hysteresis and Mullins Effect of Tough Double-Network Hydrogels. *Macromolecules* **2007**, *40* (8), 2919–2927.

(28) Sakai, T.; Matsunaga, T.; Yamamoto, Y.; Ito, C.; Yoshida, R.; Suzuki, S.; Sasaki, N.; Shibayama, M.; Chung, U.-I. Design and Fabrication of a High-Strength Hydrogel with Ideally Homogeneous Network Structure from Tetrahedron-like Macromonomers. *Macromolecules* **2008**, *41* (14), 5379–5384.

(29) Davis, D. A.; Hamilton, A.; Yang, J.; Cremar, L. D.; Van Gough, D.; Potisek, S. L.; Ong, M. T.; Braun, P. V.; Martínez, T. J.; White, S. R.; Moore, J. S.; Sottos, N. R. Force-Induced Activation of Covalent Bonds in Mechanoresponsive Polymeric Materials. *Nature* **2009**, *459* (7243), 68–72.

(30) Ducrot, E.; Chen, Y.; Bulters, M.; Sijbesma, R. P.; Creton, C. Toughening Elastomers with Sacrificial Bonds and Watching Them Break. *Science* **2014**, *344* (6180), 186–189.

(31) Imato, K.; Kanehara, T.; Ohishi, T.; Nishihara, M.; Yajima, H.; Ito, M.; Takahara, A.; Otsuka, H. Mechanochromic Dynamic Covalent Elastomers: Quantitative Stress Evaluation and Autonomous Recovery. *ACS Macro Lett.* **2015**, *4* (11), 1307–1311.

(32) Lin, N.; Liu, X. Y. Correlation between Hierarchical Structure of Crystal Networks and Macroscopic Performance of Mesoscopic Soft Materials and Engineering Principles. *Chem. Soc. Rev.* **2015**, *44* (21), 7881–7915.

(33) Neal, J. A.; Mozhdehi, D.; Guan, Z. Enhancing Mechanical Performance of a Covalent Self-Healing Material by Sacrificial Noncovalent Bonds. *J. Am. Chem. Soc.* **2015**, *137* (14), 4846–4850.

(34) Filippidi, E.; Cristiani, T. R.; Eisenbach, C. D.; Waite, J. H.; Israelachvili, J. N.; Ahn, B. K.; Valentine, M. T. Toughening Elastomers Using Mussel-Inspired Iron-Catechol Complexes. *Science* **2017**, *358* (6362), 502–505.

(35) Matsuda, T.; Kawakami, R.; Namba, R.; Nakajima, T.; Gong, J. P. Mechanoresponsive Self-Growing Hydrogels Inspired by Muscle Training. *Science* **2019**, *363* (6426), 504–508.

(36) Li, X.; Nakagawa, S.; Tsuji, Y.; Watanabe, N.; Shibayama, M. Polymer Gel with a Flexible and Highly Ordered Three-Dimensional Network Synthesized via Bond Percolation. *Sci. Adv.* **2019**, *5* (12), eaax8647.

(37) Kato, S.; Furukawa, S.; Aoki, D.; Goseki, R.; Oikawa, K.; Tsuchiya, K.; Shimada, N.; Maruyama, A.; Numata, K.; Otsuka, H. Crystallization-Induced Mechanofluorescence for Visualization of Polymer Crystallization. *Nature Commun.* **2021**, *12* (1), 126.

(38) Liu, C.; Morimoto, N.; Jiang, L.; Kawahara, S.; Noritomi, T.; Yokoyama, H.; Mayumi, K.; Ito, K. Tough Hydrogels with Rapid Self-Reinforcement. *Science* **2021**, *372* (6546), 1078–1081.

(39) Fujiyabu, T.; Sakumichi, N.; Katashima, T.; Liu, C.; Mayumi, K.; Chung, U.-I.; Sakai, T. Tri-Branched Gels: Rubbery Materials with the Lowest Branching Factor Approach the Ideal Elastic Limit. *Sci. Adv.* **2022**, *8* (14), eabk0010.

(40) Ohira, M.; Katashima, T.; Naito, M.; Aoki, D.; Yoshikawa, Y.; Iwase, H.; Takata, S.-I.; Miyata, K.; Chung, U.-I.; Sakai, T.; Shibayama, M.; Li, X. Star-Polymer-DNA Gels Showing Highly Predictable and Tunable Mechanical Responses. *Adv. Mater.* **2022**, *34* (13), e2108818.

(41) Creton, C.; Kramer, E. J.; Hui, C. Y.; Brown, H. R. Failure Mechanisms of Polymer Interfaces Reinforced with Block Copolymers. *Macromolecules* **1992**, *25* (12), 3075–3088.

(42) Lin, L.; Argon, A. S. Structure and Plastic Deformation of Polyethylene. *J. Mater. Sci.* **1994**, *29* (2), 294–323.

(43) Qi, H. J.; Boyce, M. C. Stress–Strain Behavior of Thermoplastic Polyurethanes. *Mech. Mater.* **2005**, *37* (8), 817–839.

(44) Eichhorn, S. J.; Dufresne, A.; Aranguren, M.; Marcovich, N. E.; Capadona, J. R.; Rowan, S. J.; Weder, C.; Thielemans, W.; Roman, M.; Renneckar, S.; Gindl, W.; Veigel, S.; Keckes, J.; Yano, H.; Abe, K.; Nogi, M.; Nakagaito, A. N.; Mangalam, A.; Simonsen, J.; Benight, A. S.; Bismarck, A.; Berglund, L. A.; Peijs, T. Review: Current International Research into Cellulose Nanofibres and Nanocomposites. *J. Mater. Sci.* **2010**, *45* (1), 1–33.

(45) Katz, J. R. Röntgenspektrographische Untersuchungen am gedehnten Kautschuk und ihre mögliche Bedeutung für das Problem der Dehnungseigenschaften dieser Substanz. *Sci. Nat.* **1925**, *13* (19), 410–416.

(46) Keller, A.; Machin, M. J. Oriented Crystallization in Polymers. *J. Macromol. Sci. Phys.* **1967**, *1* (1), 41–91.

(47) Yeh, G. S. Y.; Hong, K. Z. Strain-Induced Crystallization, Part III: Theory. *Polym. Eng. Sci.* **1979**, *19* (6), 395–400.

(48) Huneau, B. Strain-Induced Crystallization of Natural Rubber: A Review of x-Ray Diffraction Investigations. *Rubber Chem. Technol.* **2011**, *84* (3), 425–452.

(49) Fukahori, Y. "Mechanism of the Self-Reinforcement of Cross-Linked NR Generated through the Strain-Induced Crystallization." *Polymer* **2010**, *51* (7), 1621–1631.

(50) Rault, J.; Marchal, J.; Judeinstein, P.; Albouy, P. A. Stress-Induced Crystallization and Reinforcement in Filled Natural Rubbers: 2H NMR Study. *Macromolecules* **2006**, *39* (24), 8356–8368.

(51) Zhu, P.; Zhou, C.; Wang, Y.; Sauer, B.; Hu, W.; Dong, X.; Wang, D. Reversible–Irreversible Transition of Strain-Induced Crystallization in Segmented Copolymers: The Critical Strain and Chain Conformation. *ACS Appl. Polym. Mater.* **2021**, *3* (7), 3576–3585.

(52) Zhu, P.; Dong, X.; Wang, D. Strain-Induced Crystallization of Segmented Copolymers: Deviation from the Classic Deformation Mechanism. *Macromolecules* **2017**, *50* (10), 3911–3921.

(53) Candau, N.; Laghmach, R.; Chazeau, L.; Chenal, J.-M.; Gauthier, C.; Biben, T.; Munch, E. Strain-Induced

Crystallization of Natural Rubber and Cross-Link Densities Heterogeneities. *Macromolecules* **2014**, *47* (16), 5815–5824.

(54) Brüning, K.; Schneider, K.; Roth, S. V.; Heinrich, G. Kinetics of Strain-Induced Crystallization in Natural Rubber Studied by WAXD: Dynamic and Impact Tensile Experiments. *Macromolecules* **2012**, *45* (19), 7914–7919.

(55) Toki, S.; Sics, I.; Ran, S.; Liu, L.; Hsiao, B. S.; Murakami, S.; Senoo, K.; Kohjiya, S. New Insights into Structural Development in Natural Rubber during Uniaxial Deformation by in Situ Synchrotron X-Ray Diffraction. *Macromolecules* **2002**, *35* (17), 6578–6584.

(56) Siesler, H. W. The Characterization of Polymer Deformation by Rheo-Optical Fourier-Transform Infrared Spectroscopy. *Makromol. Chem.* **1992**, *53* (1), 89–103.

(57) Osumi, R.; Yasui, T.; Tanaka, R.; Mai, T.-T.; Takagi, H.; Shimizu, N.; Tsunoda, K.; Sakurai, S.; Urayama, K. Impact of Strain-Induced Crystallization on Fast Crack Growth in Stretched Cis-1,4-Polyisoprene Rubber. *ACS Macro Lett.* **2022**, *11* (6), 747–752.

(58) Pritchard, R. H.; Lava, P.; Debruyne, D.; Terentjev, E. M. Precise Determination of the Poisson Ratio in Soft Materials with 2D Digital Image Correlation. *Soft Matter* **2013**, *9* (26), 6037.

(59) Jerabek, M.; Major, Z.; Lang, R. W. Strain Determination of Polymeric Materials Using Digital Image Correlation. *Polym. Test.* **2010**, *29* (3), 407–416.

(60) Pan, B.; Qian, K.; Xie, H.; Asundi, A. Two-Dimensional Digital Image Correlation for in-Plane Displacement and Strain Measurement: A Review. *Meas. Sci. Technol.* **2009**, *20* (6), 062001.

(61) Chen, Y.; Mellot, G.; van Luijk, D.; Creton, C.; Sijbesma, R. P. Mechanochemical Tools for Polymer Materials. *Chem. Soc. Rev.* **2021**, *50* (6), 4100–4140.

(62) Lloyd, E. M.; Vakil, J. R.; Yao, Y.; Sottos, N. R.; Craig, S. L. Covalent Mechanochemistry and Contemporary Polymer Network Chemistry: A Marriage in the Making. *J. Am. Chem. Soc.* **2023**, *145* (2), 751–768.

(63) Willis-Fox, N.; Watchorn-Rokutan, E.; Rognin, E.; Daly, R. Technology Pull: Scale-up of Polymeric Mechanochemical Force Sensors. *Trends Chem.* **2023**, *5* (6), 415–431.

(64) O'Neill, R. T.; Boulatov, R. The Many Flavours of Mechanochemistry and Its Plausible Conceptual Underpinnings. *Nat. Rev. Chem.* **2021**, *5* (3), 148–167.

(65) Stratigaki, M.; Göstl, R. Methods for Exerting and Sensing Force in Polymer Materials Using Mechanophores. *ChemPlusChem* **2020**, *85* (6), 1095–1103.

(66) Chen, Z.; Mercer, J. A. M.; Zhu, X.; Romaniuk, J. A. H.; Pfattner, R.; Cegelski, L.; Martinez, T. J.; Burns, N. Z.; Xia, Y. Mechanochemical Unzipping of Insulating Polyladderene to Semiconducting Polyacetylene. *Science* **2017**, *357* (6350), 475–479.

(67) Li, J.; Nagamani, C.; Moore, J. S. Polymer Mechanochemistry: From Destructive to Productive. *Acc. Chem. Res.* **2015**, *48* (8), 2181–2190.

(68) Ciardelli, F.; Ruggeri, G.; Pucci, A. Dye-Containing Polymers: Methods for Preparation of Mechanochromic Materials. *Chem. Soc. Rev.* **2013**, *42* (3), 857–870.

(69) Chen, X.-X.; Bayard, F.; Gonzalez-Sanchis, N.; Pamungkas, K. K. P.; Sakai, N.; Matile, S. Fluorescent Flippers: Small-Molecule Probes to Image Membrane Tension in Living Systems. *Angew. Chem. Int. Ed.* **2023**, *62* (20), e202217868.

(70) Matellan, C.; Del Río Hernández, A. E. Where No Hand Has Gone before: Probing Mechanobiology at the Cellular Level. *ACS Biomater. Sci. Eng.* **2019**, *5* (8), 3703–3719.

(71) Liu, Y.; Galior, K.; Ma, V. P.-Y.; Salaita, K. Molecular Tension Probes for Imaging Forces at the Cell Surface. *Acc. Chem. Res.* **2017**, *50* (12), 2915–2924.

(72) Freikamp, A.; Cost, A.-L.; Grashoff, C. The Piconewton Force Awakens: Quantifying Mechanics in Cells. *Trends Cell Biol.* **2016**, *26* (11), 838–847.

(73) Iskratsch, T.; Wolfenson, H.; Sheetz, M. P. Appreciating Force and Shape—the Rise of Mechanotransduction in Cell Biology. *Nat. Rev. Mol. Cell Biol.* **2014**, *15* (12), 825–833.

(74) Brockman, J. M.; Blanchard, A. T.; Pui-Yan, V., Ma; Derricotte, W. D.; Zhang, Y.; Fay, M. E.; Lam, W. A.; Evangelista, F. A.; Mattheyses, A. L.; Salaita, K. Mapping the 3D Orientation of Piconewton Integrin Traction Forces. *Nat. Methods* **2018**, *15* (2), 115–118.

(75) Stabley, D. R.; Jurchenko, C.; Marshall, S. S.; Salaita, K. S. Visualizing Mechanical Tension across Membrane Receptors with a Fluorescent Sensor. *Nat. Methods* **2011**, *9* (1), 64–67.

(76) Grashoff, C.; Hoffman, B. D.; Brenner, M. D.; Zhou, R.; Parsons, M.; Yang, M. T.; McLean, M. A.; Sligar, S. G.; Chen, C. S.; Ha, T.; Schwartz, M. A. Measuring Mechanical Tension across Vinculin Reveals Regulation of Focal Adhesion Dynamics. *Nature* **2010**, *466* (7303), 263–266.

(77) Barbee, M. H.; Kouznetsova, T.; Barrett, S. L.; Gossweiler, G. R.; Lin, Y.; Rastogi, S. K.; Brittain, W. J.; Craig, S. L. Substituent Effects and Mechanism in a Mechanochemical Reaction. *J. Am. Chem. Soc.* **2018**, *140* (40), 12746–12750.

(78) Gossweiler, G. R.; Kouznetsova, T. B.; Craig, S. L. Force-Rate Characterization of Two Spiropyran-Based Molecular Force Probes. *J. Am. Chem. Soc.* **2015**, *137* (19), 6148–6151.

(79) Horst, M.; Yang, J.; Meisner, J.; Kouznetsova, T. B.; Martínez, T. J.; Craig, S. L.; Xia, Y. Understanding the Mechanochemistry of Ladder-Type Cyclobutane Mechanophores by Single Molecule Force Spectroscopy. *J. Am. Chem. Soc.* **2021**, *143* (31), 12328–12334.

(80) Ghanem, M. A.; Basu, A.; Behrou, R.; Boechler, N.; Boydston, A. J.; Craig, S. L.; Lin, Y.; Lynde, B. E.; Nelson, A.; Shen, H.; Storti, D. W. The Role of Polymer Mechanochemistry in Responsive Materials and Additive Manufacturing. *Nat. Rev. Mater.* **2020**, *6* (1), 84–98.

(81) Izak-Nau, E.; Campagna, D.; Baumann, C.; Göstl, R. Polymer Mechanochemistry-Enabled Pericyclic Reactions. *Polym. Chem.* **2020**, *11* (13), 2274–2299.

(82) Hu, H.; Ma, Z.; Jia, X. Reaction Cascades in Polymer Mechanochemistry. *Mater. Chem. Front.* **2020**, *4* (11), 3115–3129.

(83) Brown, C. L.; Craig, S. L. Molecular Engineering of Mechanophore Activity for Stress-Responsive Polymeric Materials. *Chem. Sci.* **2015**, *6* (4), 2158–2165.

(84) Wang, S.; Hu, Y.; Kouznetsova, T. B.; Sapir, L.; Chen, D.; Herzog-Arbeitman, A.; Johnson, J. A.; Rubinstein, M.; Craig, S. L. Facile Mechanochemical Cycloreversion of Polymer Cross-Linkers Enhances Tear Resistance. *Science* **2023**, *380* (6651), 1248–1252.

(85) Watabe, T.; Aoki, D.; Otsuka, H. Polymer-Network Toughening and Highly Sensitive Mechanochromism via a Dynamic Covalent Mechanophore and a Multinetwork Strategy. *Macromolecules* **2022**, *55* (13), 5795–5802.

(86) Imato, K.; Nishihara, M.; Kanehara, T.; Amamoto, Y.; Takahara, A.; Otsuka, H. Self-Healing of Chemical Gels Cross-Linked by Diarylbibenzofuranone-Based Trigger-Free Dynamic Covalent Bonds at Room Temperature. *Angew. Chem. Int. Ed.* **2012**, *51* (5), 1138–1142.

(87) Zheng, K.; Zhang, Y.; Li, B.; Granick, S. Phosphorescent Extensophores Expose Elastic Nonuniformity in Polymer Networks. *Nat. Commun.* **2023**, *14* (1), 537.

(88) Filonenko, G. A.; Sun, D.; Weber, M.; Müller, C.; Pidko, E. A. Multicolor Organometallic Mechanophores for Polymer Imaging Driven by Exciplex Level Interactions. *J. Am. Chem. Soc.* **2019**, *141* (24), 9687–9692.

(89) Filonenko, G. A.; Lugger, J. A. M.; Liu, C.; van Heeswijk, E. P. A.; Hendrix, M. M. R. M.; Weber, M.; Müller, C.; Hensen, E. J. M.; Sijbesma, R. P.; Pidko, E. A. Tracking Local Mechanical Impact in Heterogeneous Polymers with Direct Optical Imaging. *Angew. Chem. Int. Ed.* **2018**, *57* (50), 16385–16390.

(90) Khang, T. M.; Huang, R.; Khan, A.; Chuang, W.-T.; Quoc Nhien, P.; Cuc, T. T. K.; Hue, B. T. B.; Wei, K.-H.; Li, Y.-K.; Lin, H.-C. Reversible Ratiometric Mechanochromic Fluorescence Switching in Highly Stretchable Polyurethane Elastomers with Ultratoughness Enhanced by Polyrotaxane. *ACS Mater. Lett.* **2022**, *4* (12), 2537–2546.

(91) He, S.; Stratigaki, M.; Centeno, S. P.; Dreuw, A.; Göstl, R. Tailoring the Properties of Optical Force Probes for Polymer Mechanochemistry. *Chem. Eur. J* **2021**, *27* (64), 15889–15897.

(92) Robb, M. J.; Li, W.; Gergely, R. C. R.; Matthews, C. C.; White, S. R.; Sottos, N. R.; Moore, J. S. A Robust Damage-Reporting Strategy for Polymeric Materials Enabled by Aggregation-Induced Emission. *ACS Cent. Sci.* **2016**, *2* (9), 598–603.

(93) Kotani, R.; Yokoyama, S.; Nobusue, S.; Yamaguchi, S.; Osuka, A.; Yabu, H.; Saito, S. Bridging Pico-to-Nanonewtons with a Ratiometric Force Probe for Monitoring Nanoscale Polymer Physics before Damage. *Nat. Commun.* **2022**, *13* (1), 303.

(94) Yamakado, T.; Saito, S. Ratiometric Flapping Force Probe That Works in Polymer Gels. *J. Am. Chem. Soc.* **2022**, *144* (6), 2804–2815.

(95) Yamakado, T.; Otsubo, K.; Osuka, A.; Saito, S. Compression of a Flapping Mechanophore Accompanied by Thermal Void Collapse in a Crystalline Phase. *J. Am. Chem. Soc.* **2018**, *140* (20), 6245–6248.

(96) Yuan, C.; Saito, S.; Camacho, C.; Irle, S.; Hisaki, I.; Yamaguchi, S. A π-Conjugated System with Flexibility and Rigidity That Shows Environment-Dependent RGB Luminescence. *J. Am. Chem. Soc.* **2013**, *135* (24), 8842–8845.

(97) Kotani, R.; Sotome, H.; Okajima, H.; Yokoyama, S.; Nakaike, Y.; Kashiwagi, A.; Mori, C.; Nakada, Y.; Yamaguchi, S.; Osuka, A.; Sakamoto, A.; Miyasaka, H.; Saito, S. Flapping Viscosity Probe That Shows Polarity-Independent Ratiometric Fluorescence. *J. Mater. Chem. C* **2017**, *5* (21), 5248–5256.

(98) Paul, S.; Kitakado, H.; Suga, K.; Kotani, R.; Dey, N.; Matito, E.; Venkatramani, R.; Saito, S.; Dasgupta, J. Triplet Conformation in Chromophore-Fused Cyclooctatetraene Dyes. *J. Mater. Chem. C* **2023**. https://doi.org/10.1039/d3tc02151c.

(99) Hertel, R.; Maftuhin, W.; Walter, M.; Sommer, M. Conformer Ring Flip Enhances Mechanochromic Performance of Ansa-Donor-Acceptor-Donor Mechanochromic Torsional Springs. *J. Am. Chem. Soc.* **2022**, *144* (48), 21897–21907.

(100) Raisch, M.; Maftuhin, W.; Walter, M.; Sommer, M. A Mechanochromic Donor-Acceptor Torsional Spring. *Nat. Commun.* **2021**, *12* (1), 4243.

(101) Qian, H.; Purwanto, N. S.; Ivanoff, D. G.; Halmes, A. J.; Sottos, N. R.; Moore, J. S. Fast, Reversible Mechanochromism of Regioisomeric Oxazine Mechanophores: Developing in Situ Responsive Force Probes for Polymeric Materials. *Chem* **2021**, *7* (4), 1080–1091.

(102) Muramatsu, T.; Okado, Y.; Traeger, H.; Schrettl, S.; Tamaoki, N.; Weder, C.; Sagara, Y. Rotaxane-Based Dual Function Mechanophores Exhibiting Reversible and Irreversible Responses. *J. Am. Chem. Soc.* **2021**, *143* (26), 9884–9892.

(103) Sagara, Y.; Karman, M.; Seki, A.; Pannipara, M.; Tamaoki, N.; Weder, C. Rotaxane-Based Mechanophores Enable Polymers with Mechanically Switchable White Photoluminescence. *ACS Cent. Sci.* **2019**, *5* (5), 874–881.

(104) Sagara, Y.; Karman, M.; Verde-Sesto, E.; Matsuo, K.; Kim, Y.; Tamaoki, N.; Weder, C. Rotaxanes as Mechanochromic Fluorescent Force Transducers in Polymers. *J. Am. Chem. Soc.* **2018**, *140* (5), 1584–1587.

(105) Dal Molin, M.; Verolet, Q.; Colom, A.; Letrun, R.; Derivery, E.; Gonzalez-Gaitan, M.; Vauthey, E.; Roux, A.; Sakai, N.; Matile, S. Fluorescent Flippers for Mechanosensitive Membrane Probes. *J. Am. Chem. Soc.* **2015**, *137* (2), 568–571.

(106) Gossweiler, G. R.; Hewage, G. B.; Soriano, G.; Wang, Q.; Welshofer, G. W.; Zhao, X.; Craig, S. L. Mechanochemical Activation of Covalent Bonds in Polymers with Full and Repeatable Macroscopic Shape Recovery. *ACS Macro Lett.* **2014**, *3* (3), 216–219.

(107) Black, A. L.; Lenhardt, J. M.; Craig, S. L. From Molecular Mechanochemistry to Stress-Responsive Materials. *J. Mater. Chem.* **2011**, *21* (6), 1655–1663.

(108) Filonenko, G. A.; Khusnutdinova, J. R. Dynamic Phosphorescent Probe for Facile and Reversible Stress Sensing. *Adv. Mater.* **2017**, *29* (22), 1700563.

(109) Beyer, M. K.; Clausen-Schaumann, H. Mechanochemistry: The Mechanical Activation of Covalent Bonds. *Chem. Rev.* **2005**, *105* (8), 2921–2948.

(110) Goto, Y.; Omagari, S.; Sato, R.; Yamakado, T.; Achiwa, R.; Dey, N.; Suga, K.; Vacha, M.; Saito, S. Dynamic Polymer Free Volume Monitored by Single-Molecule Spectroscopy of a Dual Fluorescent Flapping Dopant. *J. Am. Chem. Soc.* **2021**, *143* (35), 14306–14313.

(111) Suga, K.; Yamakado, T.; Saito, S. Nitrogen-Substitution in the Flapping Wings of Cyclooctatetraene-Fused Molecules. *Bull. Chem. Soc. Jpn* **2021**, *94* (7), 1999–2002.

(112) Crenshaw, B. R.; Weder, C. Self-Assessing Photoluminescent Polyurethanes. *Macromolecules* **2006**, *39* (26), 9581–9589.

(113) Ahmed, S. A.; Zang, Z. W.; Yoo, K. M.; Ali, M. A.; Alfano, R. R. Effect of Multiple Light Scattering and Self-Absorption on the Fluorescence and Excitation Spectra of Dyes in Random Media. *Appl. Opt.* **1994**, *33* (13), 2746–2750.

(114) Toki, S.; Sics, I.; Hsiao, B. S.; Tosaka, M.; Poompradub, S.; Ikeda, Y.; Kohjiya, S. Probing the Nature of Strain-Induced Crystallization in Polyisoprene Rubber by Combined Thermomechanical and in Situ X-Ray Diffraction Techniques. *Macromolecules* **2005**, *38* (16), 7064–7073.

(115) Lu, X. Crystallization Orientation and Relaxation in Uniaxially Drawn Poly(Ethylene Terephthalate). *Polymer* **2001**, *42* (19), 8055–8067.

Table of Contents artwork